



OPEN

## Clinical and simulated impact of intraocular lens tilt and decentration based on real-world data and optical simulation

Gonzalo Velarde-Rodríguez<sup>1,2</sup>✉, Nicolás Alejandro-Alba<sup>1,2</sup>, Azahara Sánchez-Lozano<sup>1</sup>, Luis García-Onrubia<sup>1</sup>, Ignacio Jiménez-Alfaro Morote<sup>1,2</sup> & Miguel Faria-Ribeiro<sup>3</sup>

The aim of this study was to determine whether the optical degradation induced by clinically measured intraocular lens (IOL) tilt and decentration, quantified through individualized synthetic eye models, translates into measurable changes in subjective refraction or visual acuity (BCVA). We included 105 eyes implanted with monofocal aspheric IOL and measured their positioning using AS-OCT. These data were used to reconstruct each eye in optical simulation software and evaluate four scenarios: aligned, decentered, tilted, and combined decentration and tilt. For each case, we calculated wavefront aberrations, three objective refractions, and predicted visual acuity from the radial MTF. The average IOL tilt was  $5.19 \pm 1.28^\circ$  and decentration was  $0.25 \pm 0.13$  mm. Coma RMS increased from  $0.00 \mu\text{m}$  in the aligned model to  $0.26 \pm 0.09 \mu\text{m}$  in the most altered scenario ( $p < 0.001$ ), and VSX decreased from  $0.80 \pm 0.11$  to  $0.35 \pm 0.17$ . Despite this optical degradation, BCVA remained unaffected, with a mean of  $0.00 \pm 0.05$  LogMAR, and no significant correlation was found with tilt or decentration. The best agreement between simulated and clinical refraction was observed when both tilt and decentration were included. These results suggest that moderate IOL misalignment degrades optical quality without compromising visual acuity in monofocal IOLs, but further studies are needed for multifocal designs.

The influence of intraocular lens (IOL) tilt on postoperative refraction was clinically described during the development of the first IOL power calculation formulas<sup>1–3</sup>. Later, this issue and the consequences of IOL misalignment were elegantly explained using paraxial optics<sup>4–6</sup>. As newer formulas and toric IOLs were developed and residual refraction improved, this topic gained even more importance<sup>7,8</sup>. The sensitivity of multifocal and extended depth of focus (EDOF) IOLs to misalignment prompted researchers to investigate the topic using optical bench setups<sup>8,9</sup> and ocular wavefront measurements<sup>10,11</sup>. More recently, ray-tracing software has been used to simulate synthetic ocular models to evaluate IOL tilt and decentration<sup>12,13</sup>.

Scheimpflug imaging and anterior segment optical coherence tomography (AS-OCT) have enabled clinical evaluation of IOL tilt and decentration. Studies report mean tilt values between  $2^\circ$  and  $5^\circ$ , depending on factors such as axial length, IOL haptics, capsular tension ring use, and preoperative crystalline lens tilt<sup>14,15</sup>. These factors also influence the sagittal and meridional displacement of the IOL, with typical decentration values around  $0.2$ – $0.3$  mm<sup>16</sup>. Both tilt and decentration can impair visual quality by inducing high-order aberrations (HOAs), and in more extreme cases, may reduce visual acuity (VA). Some studies suggest that decentration has a more significant impact on vision than tilt, although both are influenced by IOL design<sup>17,18</sup>. The visual impact of decentering a spherical IOL is less pronounced than with aspheric designs; however, tilt appears to affect both types similarly<sup>19,20</sup>. IOL tilt is more strongly correlated with coma-like aberrations, while both tilt and decentration contribute to induced astigmatism<sup>21,22</sup>.

As premium IOLs evolve rapidly, more sophisticated designs demand a deeper understanding of ocular optics. While optical bench simulations have provided valuable insights into IOL misalignment, and clinical studies have documented its effects on visual acuity, few studies have combined both perspectives to assess the impact on ocular aberrations comprehensively. The aim of this study is to determine whether the optical degradation induced by IOL tilt and decentration, quantified using individualized synthetic eye models built

<sup>1</sup>Ophthalmology Department, Fundación Jiménez Díaz University Hospital, C/ Avenida Reyes Católicos, 2, Madrid C.P. 28040, Spain. <sup>2</sup>IIS-FJD, UAM: Health Research Institute Fundación Jiménez Díaz, Madrid, Spain. <sup>3</sup>Physics Center of Minho and Porto Universities, School of Sciences, University of Minho, Braga, Portugal. ✉email: gonzalo.velarde@quironsalud.es

from real postoperative data, translates into measurable clinical changes in subjective refraction and BCVA. In addition, we evaluated the internal consistency of the model by comparing the objective prescriptions derived from ray-tracing analysis with the subjective refraction obtained in each patient.

## Methods

### Settings

This cross-sectional study was conducted at Fundación Jiménez Díaz University Hospital between November 2023 and June 2024. The local institutional review board (Comité de Etica de la Investigación Fundación Jiménez Diaz. Code: PIC204-24) approved the study protocol, which complies with the tenets of the Declaration of Helsinki. Written informed consent was obtained from all subjects prior to the commencement of the study, following an explanation of the nature and possible consequences of the study.

### Patient eligibility

Patients who underwent uneventful cataract surgery of both eyes and implanted with Clareon® CNAT0 with a minimum follow-up of 3 months were included. The exclusion criteria comprehend amblyopia, retinal or corneal or any other ocular disease that could affect the patient's vision performance. Also, any patient with history of ocular surgery such as refractive surgery or interventions that could affect the capsule-bag integrity like Nd-YAG capsulotomy was excluded.

### Measurement protocol

Subjective refraction to obtain the best corrected visual acuity (BCVA) was performed by the same experienced optometrist (ASL) using ETDRS chart. One drop of tropicamide (1%) was instilled for the next measurements.

Postoperative biometry using IOL-Master 700 (Carl Zeiss Meditec, AG, Jena, Germany, version 1.90.33.04) was used to acquire axial length. Patients anterior segment was measured with AS-OCT CASIA II (TOMEY corp, Nagoya, Japan, version 50.6B.07) using the cataract protocol examination. Only measurements labeled as OK by the instrument were included in this study. IOL edge detection was performed by a researcher (GVR) using the semi-trace method included in the AS-OCT software.

### IOL parametrization

The anterior radii of curvature and central thickness of each implanted IOL were measured using the AS-OCT software. Although the software also reports the posterior radius of curvature, accurate identification of the posterior IOL surface was often impaired by the proximity of the posterior capsule, leading to acquisition errors.

To address this limitation, it was assumed that the labeled paraxial power of IOL matched its nominal value. Based on this assumption and using the refractive index provided by the manufacturer ( $Nd = 1.55$ , at  $35^\circ\text{C}$ ), the posterior radius of curvature was calculated such that the combination of anterior radius, central thickness, and material index would result in the labeled paraxial power.

Each IOL's anterior surface was then modeled as a fourth order even asphere, excluding the 2nd-order term. The conic constant ( $k$ ) and fourth-order aspheric coefficient ( $a_4$ ) were optimized in Zemax OpticStudio to ensure that the IOL corrected  $-0.20\text{ }\mu\text{m}$  of fourth-order corneal spherical aberration (Zernike term) in a physiological model eye, assuming a  $6.0\text{ mm}$  entrance pupil.

### Synthetic eye model and simulating different scenarios

Ansys Zemax OpticStudio (v 22.1) was used to build the eye model. Coordinates breaks were used to include pupil decentration, IOL tilt and decentration and corneal angle shift of the principal axes (Z-axis tilt). The anterior and posterior corneal surface were included as a biconic surface with data from IOL Master 700 principal meridians (setting conic constant to zero). The iris was represented by a stop surface of pupil's patient diameter and situated  $0.75\text{ mm}$  before the IOL anterior surface. IOL anterior surface was described as a fourth order even asphere and a posterior standard surface, adhering to the data collected by the AS-OCT and the IOL power labelled by manufacturer. The system setting was adjusted for a wavelength of  $550\text{ nm}$  with no field modification. The selected pupil for the analysis was  $4\text{ mm}$ . The refractive indices used in this model were  $1.3752$  for the cornea and  $1.336$  for the aqueous and vitreous humors. More information is available in Fig. 1.

Four scenarios were simulated using this eye model. The first situation was with the IOL totally aligned. In the second one, the measured IOL decentration (AS-OCT) was introduced, then the IOL tilt was set and finally the IOL decentration was set to zero. Therefore, four scenarios were evaluated as "Aligned", "Decentration", "Decentration + tilt" and "Tilted" respectively. The wavefront phase and its associated Zernike coefficients values (up to sixth order) were collected for each situation.

### Objective synthetic refraction

A total of three refractions for each of the described scenarios were obtained for each patient derived from the synthetic ocular wavefront. Two objective refractions were directly obtained from the Zernike coefficient values: minimum root mean square (MinRMS) and paraxial curvature matching (PCM)<sup>23</sup>. Another refraction was calculated by maximizing the retinal image quality weighted by a neural function<sup>24</sup>. The selected metric was the visual strehl in the special domain (VSX). This was performed using an iterative process of testing lenses with the aberration map and maximizing the metric value. The following equation describes how we calculate this metric:

$$VSX = \frac{\iint PSF(x, y) * iCSF(x, y) dx dy}{\iint PSF_{DL}(x, y) * iCSF(x, y) dx dy}$$

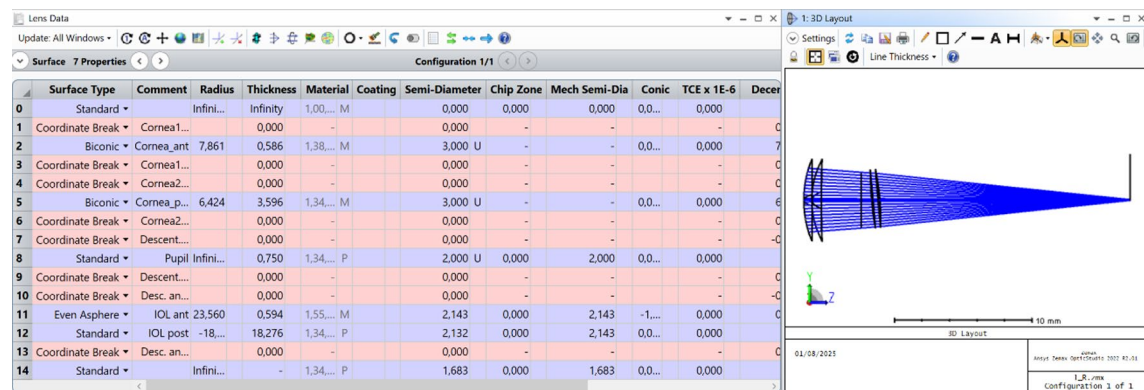


**Fig. 1.** Example for the first analyzed eye included in this study, revealing the general settings to build the synthetic eye model.

Where PSF is the point spread function and the iCSF is the inverse fourier transform of the contrast sensitivity function (CSF)<sup>25</sup>.

The optimizing process was carried out testing a combination of sphero-cylindrical lenses with a range from -3 to 3 D in steps of 0.25 D. The step for the refractive axis was 5°, from 0 to 175 degrees. These values were converted into power vectors ( $M$ ,  $J_0$  and  $J_{45}$ ) and finally into their equivalent Zernike coefficients  $Z(2,0)$ ,  $Z(2,-2)$  and  $Z(2,2)$ . These variables were converted into wavefront error in microns and added to the original ocular wavefront calculating the new value of the VSX. We selected the sphero-cylindrical prescription that maximize the VSX value.

### Internal consistency analysis of the synthetic model

To assess the consistency of the eye model, the predicted visual ( $VA_{pred}$ ) acuity was estimated by identifying the intersection between the radial modulation transfer function (MTFr) and the contrast sensitivity threshold<sup>26</sup>. Additionally, the objective prescriptions were derived from the scenario IOL decentration and tilt, which replicates the actual clinical setting in the synthetic eye model. This comparison was evaluated twofold, with the subtraction (subjective prescription - objective prescription) and by the Bland-Altman agreement analysis method.

### Impact of IOL Tilt and decentration in visual performance

We evaluated this question using two complementary approaches: variables derived from the synthetic eye model, which describe the optical impact of misalignment, and clinical measurements obtained from the same eyes.

The synthetic eye model allows the statistical comparison of the image quality metrics such as VSX or the optical aberrations (RMS astigmatism and RMS Coma) for the different simulated scenarios ('Aligned', 'Decentration', 'Tilt' and 'Decentration and tilt'). These variable changes were assessed using ANOVA statistical tests, with p-values adjusted for multiple comparisons using the Bonferroni correction. A p-value < 0.05 was considered statistically significant after correction. The image quality metrics obtained for each scenario were compared using the Wilcoxon signed-ranked test and box and whiskers plots analysis.

Concerning the clinical measurements, we studied the IOL positioning (tilt and decentration) and BCVA. First, we performed a partial correlation analysis to determine the relationship between IOL tilt, decentration and BCVA. But also, we explore the BCVA differences between patients with high IOL tilt (more than third quartile) or decentration to those that presented low values (less than first quartile) of these variables. For that purpose, we used Mann-Whitney U test with the mentioned statistical threshold.

## Results

The demographic and clinical characteristics of the sample are summarized as follows. A total of 105 right eyes from 105 participants (53% females and 47% males) were included in this study. The mean patients age was  $73.35 \pm 8.39$  years old and follow-up period was  $9.41 \pm 4.54$  months after cataract surgery. A statistical summary of the main clinical variables is presented in Table 1. The main modulus of the vectors tilt and decentration were  $5.19 \pm 1.28^\circ$  and  $0.25 \pm 0.13$  mm, respectively. The study of the IOL tilt revealed a tendency, the nasal-superior IOL edge was shifted towards the cornea compared to the temporal edge. The maximum value for tilt was 9.3° (eye 12) and decentration was 0.83 mm (eye 36).

### Synthetic model outcomes and internal consistency

We first evaluated the agreement between simulated and clinical parameters, as this reflects the internal consistency of the synthetic model. The mean difference and 95% confidence interval (95%CI) between  $VA_{pred}$  and BCVA were  $-0.07$  95% CI(-0.09,-0.05) LogMAR. The Bland-Altman analysis showed a low and upper limit of agreement of -0.27, 0.14 LogMAR respectively (Fig. 2).

Category	Parameter	Values
Demographic	Number of patients (M-F)	105 (49-56)
	Number of eyes (R-L)	105 (105-0)
Biometrical data	Anterior corneal radius (mm)	$7.72 \pm 0.08$
	Posterior corneal radius (mm)	$6.52 \pm 0.21$
	Corneal central thickness (μm)	$543.03 \pm 31.35$
	Anterior chamber depth (mm)	$4.64 \pm 0.25$
	Pupil decentration [X, Y] (mm)	$[-0.26 \pm 0.21, -0.10 \pm 0.22]$
	Axial length (mm)	$23.57 \pm 1.09$
	IOL power (D)	$21.22 \pm 3.25$
	IOL decentration [X, Y] (mm)	$[-0.11 \pm 0.19, 0.03 \pm 0.18]$
Subjective refraction	IOL tilt [X, Y] (mm)	$[-4.77 \pm 1.40, -1.36 \pm 1.44]$
	M (D)	$-0.11 \pm 0.37$
	$J_0$ (DC)	$-0.19 \pm 0.27$
	$J_{45}$ (DC)	$-0.04 \pm 0.19$
	BCVA (LogMAR)	$0.00 \pm 0.05$

**Table 1.** Summarize the results for the demographic and clinical variables.

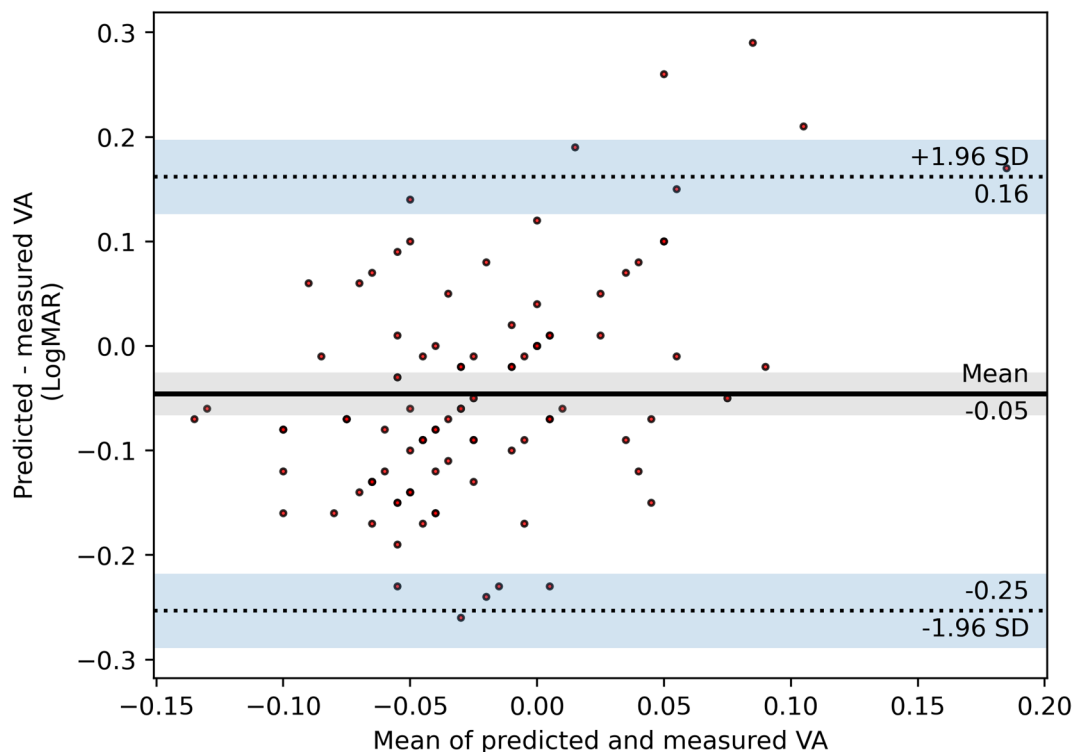


**Fig. 2.** Bland-Altman plot that shows the agreement between the predicted visual acuity using the intersection value of the threshold function and the average modulation transfer function.

We then compared the objective prescriptions derived from the synthetic wavefront with the clinical subjective refraction. The objective prescriptions calculation varies with every single scenario and their mean differences with the subjective prescription are represented in Table 2. The scenario where decentration and tilt were represented showed the minimum differences with the subjective prescription. Further details for the comparison between this scenario prescriptions and the clinical subjective prescription are extended in Fig. 3.

#### Simulated optical impact of IOL misalignment

We next quantified how tilt and decentration affected the optical quality within the synthetic model. The wavefront error changed significantly for the RMS coma ( $p < 0.001$ ), where the aligned scenario showed zero coma values and it increased its value through the next scenarios. Spherical and astigmatism aberrations slightly changed with IOL tilt and decentration.

		Aligned	Decentration	Tilt	Decentration + Tilt
MinRMS	M (D)	0.59 (0.52, 0.67)	0.55 (0.47, 0.62)	0.44 (0.36, 0.52)	0.40 (0.32, 0.48)
	$J_0$ (DC)	-0.05 (-0.11, 0.01)	-0.06 (-0.11, 0.00)	-0.11 (-0.17, -0.05)	-0.11 (-0.17, -0.05)
	$J_{45}$ (DC)	0.09 (0.05, 0.13)	0.09 (0.05, 0.13)	0.06 (0.02, 0.10)	0.08 (0.03, 0.12)
Paraxial	M (D)	0.29 (0.22, 0.37)	0.24 (0.17, 0.32)	0.14 (0.07, 0.22)	0.09 (0.01, 0.17)
	$J_0$ (DC)	-0.06 (-0.11, -0.00)	-0.06 (-0.12, -0.01)	-0.11 (-0.17, -0.06)	-0.12 (-0.18, -0.06)
	$J_{45}$ (DC)	0.09 (0.05, 0.13)	0.09 (0.05, 0.13)	0.05 (0.01, 0.10)	0.07 (0.03, 0.11)
Optimized VSX	M (D)	0.55 (0.47, 0.62)	0.46 (0.38, 0.54)	0.29 (0.20, 0.37)	0.21 (0.12, 0.29)
	$J_0$ (DC)	-0.06 (-0.11, -0.01)	-0.07 (-0.12, -0.01)	-0.08 (-0.14, -0.03)	-0.10 (-0.16, -0.04)
	$J_{45}$ (DC)	0.09 (0.05, 0.13)	0.09 (0.05, 0.13)	0.08 (0.04, 0.12)	0.11 (0.07, 0.15)

**Table 2.** Showed the mean and 95% confidence interval for each objective prescription calculated for each scenario and the subjective prescription.

We also evaluated how the simulated objective prescriptions changed across the four scenarios. While the objectives prescriptions MinRMS and PCM did not show differences when tilt and decentration were included, the M variable showed a progressive decline. In contrast this variable changed significantly for the optimized VSX prescription. Once again, the lowest value for M was found for the scenario were both, tilt and decentration were included. More details could be found in Table 3.

We further assessed how tilt and decentration influenced global image-quality metrics derived from the synthetic model. The VSX metric statistically changed between scenarios, reducing its value as long as tilt and decentration were involved. This happened for the three objective prescriptions assessed in this study and we found that IOL tilt impacts more than decentration ( $p < 0.001$ ). These differences are represented numerically in Fig. 4. Additionally, the convolution images illustrate the deterioration produced in the most extreme cases of the sample (Fig. 5).

### Clinical impact of IOL Tilt and decentration

We analyzed whether the clinical misalignment of the IOL was associated with measurable changes in BCVA. The partial Spearman correlation between IOL tilt and BCVA, controlling IOL decentration, was not statistically significant ( $r = 0.07$ , 95% CI [-0.12, 0.26],  $p = 0.48$ ). Similarly, when assessing the partial correlation between IOL decentration and BCVA while controlling for IOL tilt, no significant association was found ( $r = 0.13$ , 95% CI [-0.06, 0.32],  $p = 0.18$ ). When comparing the BCVA between groups with low and high IOL tilt, no significant differences were observed ( $p$ -value = 0.23). Same result was obtained when comparing BCVA between groups with high and low IOL decentration ( $p$ -value = 0.29).

## Discussion

This study was designed to assess whether the optical degradation resulting from IOL tilt and decentration, quantified through individualized synthetic ocular models, produces clinically measurable changes in subjective refraction or visual acuity. A secondary objective was to evaluate the internal consistency of the synthetic model by analyzing the agreement between the simulated objective prescriptions and the subjective refraction obtained in each case.

Another notable contribution of this study is the characterization of monofocal aspheric IOLs. Using their anterior radius, labeled power, and manufacturer-reported spherical aberration, we were able to implement these lenses into ray-tracing simulations. Despite the aforementioned challenges, we successfully modeled the optical aberrations of the eye and evaluated the impact of IOL tilt and decentration on visual quality. A major strength of this study is the integration of clinical data with theoretical analysis, helping to bridge the gap between basic research and clinical practice.

The study findings are in accordance with the theoretical changes produced by IOL tilt proposed by Atchison et al.<sup>5</sup>, as the M value for every prescription varies when IOL tilt and decentration are present because of the variation of the effective power of the IOL. We did not appreciate great changes in terms of the astigmatism components, probably because the IOL model selected for this study was aspherical.

Our findings show that both IOL tilt and decentration induce statistically significant coma aberrations. For IOL decentration, we found a mean value of  $0.25 \pm 0.13$  mm which induced coma aberration of  $0.11 \pm 0.06$   $\mu\text{m}$ . This result is in accordance with Perez-Gracia<sup>19</sup> which reported a coma RMS value around  $0.05\text{--}0.1 \mu\text{m}$  for  $0.25$  mm IOL decentration. In the same line, Perez-Merino et al.<sup>12</sup> reported an RMS coma from  $0.10 \mu\text{m}$  to  $0.22 \mu\text{m}$  for  $0.4$  mm decentration. Our result in coma aberration is within the range of normal reported values from other authors. These results are strongly influenced by the pupil diameter and the IOL model selected (aspherical or spherical). The mean coma aberration induced by IOL tilt ( $5.19 \pm 1.28^\circ$ ) in this study was  $0.21 \pm 0.07 \mu\text{m}$ . Other studies reported similar mean values for IOL tilt, from  $2$  to  $6$  degrees inducing a coma-like aberration from  $0.19^{22}$  to  $0.4$  microns<sup>17,19</sup>. The variability depends on several factors, such as the IOL power and design or the pupil used for the analysis.

VSX metrics proved highly sensitive to IOL tilt and decentration, showing a marked reduction in value as these misalignments increased. This behavior may be attributed to the prismatic effect caused by coma aberration on the point spread function. Interestingly, the low VSX values observed in the “tilt and decentration” scenario contrast with the good clinical BCVA outcomes.

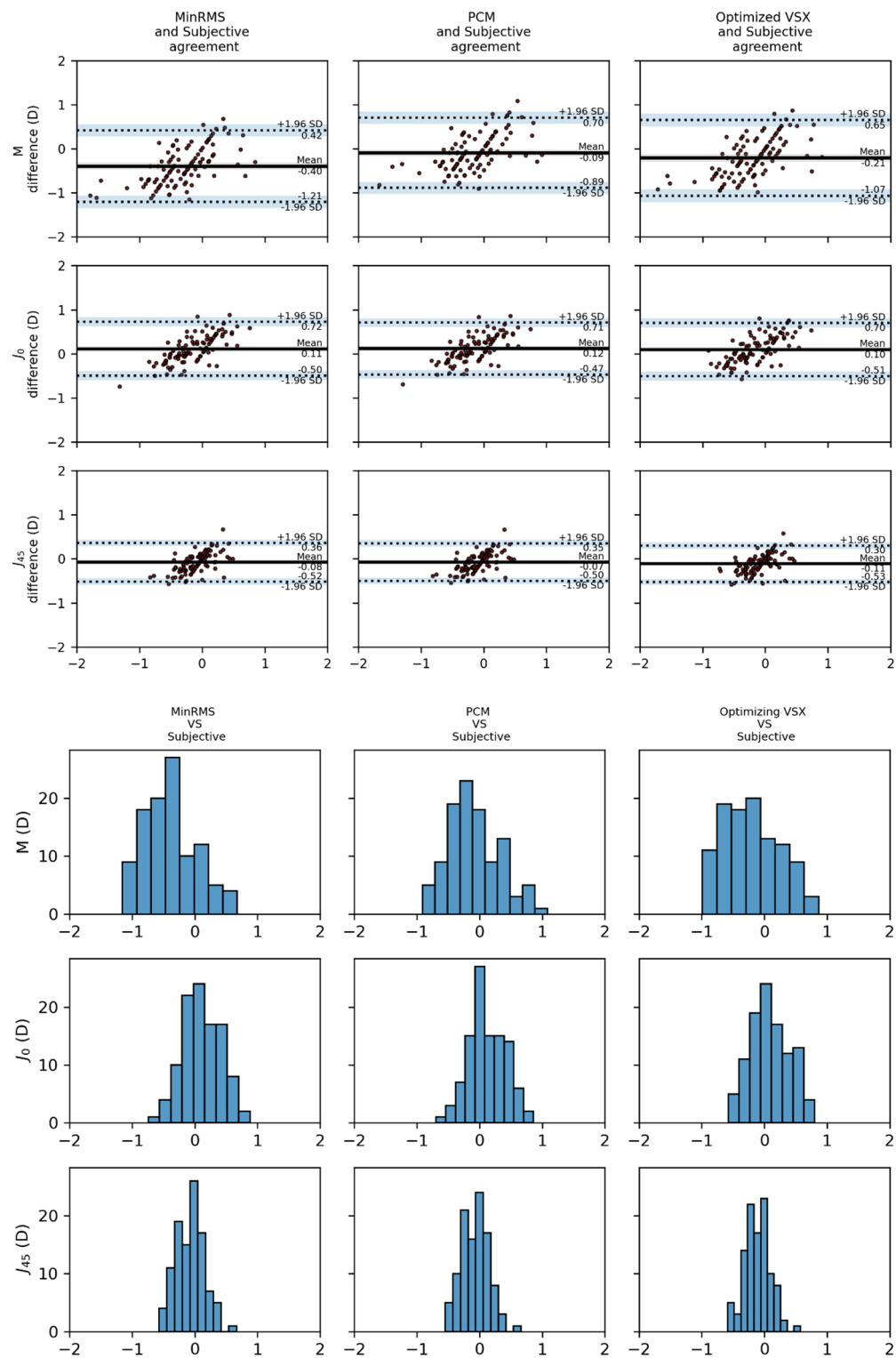


**Fig. 3.** Objective and subjective prescriptions comparative. Above the agreement using a Bland-Altman plot. Below is the histogram that represents the number of eyes (Y-axis) and the difference in diopters (X-axis) for the power vectors (M,  $J_0$  and  $J_{45}$ ).

Despite this, the correlation between the degree of tilt and decentration and the resulting BCVA was weak when an aspherical IOL was implanted, suggesting limited clinical impact. This raises the question of whether such induced aberrations could have a more pronounced effect in the context of multifocal IOLs, which are known to be more susceptible to higher-order aberrations and demand higher optical quality for optimal function.

Method	Variable	Aligned	Decentration	Tilt	Decentration + Tilt	ANOVA (corrected p-value)
Wavefront RMS	Spherical ( $\mu\text{m}$ )	$0.84 \pm 0.52$	$0.80 \pm 0.52$	$0.73 \pm 0.49$	$0.70 \pm 0.49$	1.00
	Astigmatism ( $\mu\text{m}$ )	$0.79 \pm 0.44$	$0.79 \pm 0.44$	$0.78 \pm 0.44$	$0.79 \pm 0.44$	1.00
	Coma ( $\mu\text{m}$ )	$0.00 \pm 0.00$	$0.11 \pm 0.06$	$0.21 \pm 0.07$	$0.26 \pm 0.09$	$<0.001$
MinRMS	M (D)	$-0.70 \pm 0.59$	$-0.65 \pm 0.60$	$-0.55 \pm 0.60$	$-0.50 \pm 0.60$	1.00
	$J_0$ (DC)	$-0.14 \pm 0.47$	$-0.14 \pm 0.47$	$-0.09 \pm 0.47$	$-0.08 \pm 0.48$	1.00
	$J_{45}$ (DC)	$-0.14 \pm 0.32$	$-0.14 \pm 0.32$	$-0.10 \pm 0.33$	$-0.12 \pm 0.33$	1.00
	VSX	$0.80 \pm 0.11$	$0.65 \pm 0.14$	$0.44 \pm 0.15$	$0.35 \pm 0.17$	$<0.001$
Paraxial	M (D)	$-0.40 \pm 0.57$	$-0.35 \pm 0.58$	$-0.25 \pm 0.58$	$-0.20 \pm 0.58$	0.81
	$J_0$ (DC)	$-0.14 \pm 0.45$	$-0.13 \pm 0.45$	$-0.08 \pm 0.46$	$-0.07 \pm 0.47$	1.00
	$J_{45}$ (DC)	$-0.13 \pm 0.31$	$-0.13 \pm 0.31$	$-0.10 \pm 0.32$	$-0.12 \pm 0.32$	1.00
	VSX	$0.46 \pm 0.13$	$0.44 \pm 0.12$	$0.39 \pm 0.11$	$0.33 \pm 0.12$	$<0.001$
Optimized VSX	M (D)	$-0.66 \pm 0.58$	$-0.57 \pm 0.59$	$-0.39 \pm 0.61$	$-0.32 \pm 0.62$	0.01
	$J_0$ (DC)	$-0.13 \pm 0.44$	$-0.13 \pm 0.44$	$-0.11 \pm 0.44$	$-0.10 \pm 0.47$	1.00
	$J_{45}$ (DC)	$-0.14 \pm 0.30$	$-0.13 \pm 0.31$	$-0.13 \pm 0.31$	$-0.16 \pm 0.31$	1.00
	VSX	$0.76 \pm 0.12$	$0.65 \pm 0.13$	$0.50 \pm 0.14$	$0.42 \pm 0.17$	$<0.001$

**Table 3.** Mean and standard deviation of the objective prescriptions in power vector notation and the VSX metrics value associated through different simulated scenarios. ANOVA (corrected p-value) corresponds to Bonferroni-adjusted p-values calculated across all scenario comparisons.

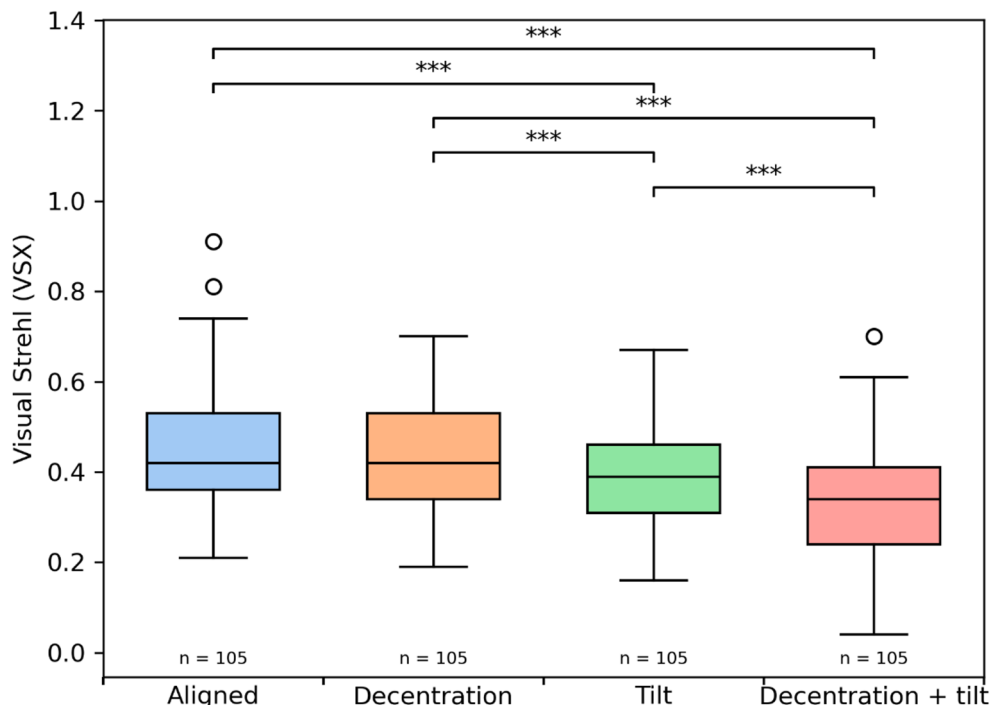


**Fig. 4.** Visual Strehl ratio (VSX) comparison across four intraocular lens (IOL) positioning scenarios: perfectly aligned, decentered, tilted, and combined decentration and tilt. All pairwise comparisons showed statistically significant differences (\*\* $p < 0.001$ ) using Wilcoxon rank sum test.

This study has several limitations, the most critical is the representation of the cornea. The IOLMaster 700 does not provide patient-specific corneal asphericity, and the corneal surfaces in the model were therefore implemented as biconics with conic constants set to zero. This approximation cannot reproduce the exact aspheric geometry of each cornea and may introduce small shifts in the absolute values of the simulated aberrations. However, the purpose of the model was to evaluate relative changes across the different misalignment scenarios, and these changes are dominated by IOL tilt and decentration. For this reason, the impact of the missing asphericity is expected to be modest and does not alter the main trends observed. Another limitation is the unavailability of exact IOL parameters from manufacturers, as such information remains proprietary. Also, our model assumes a monochromatic light source centered at 550 nm, whereas real vision involves a broad spectrum of wavelengths

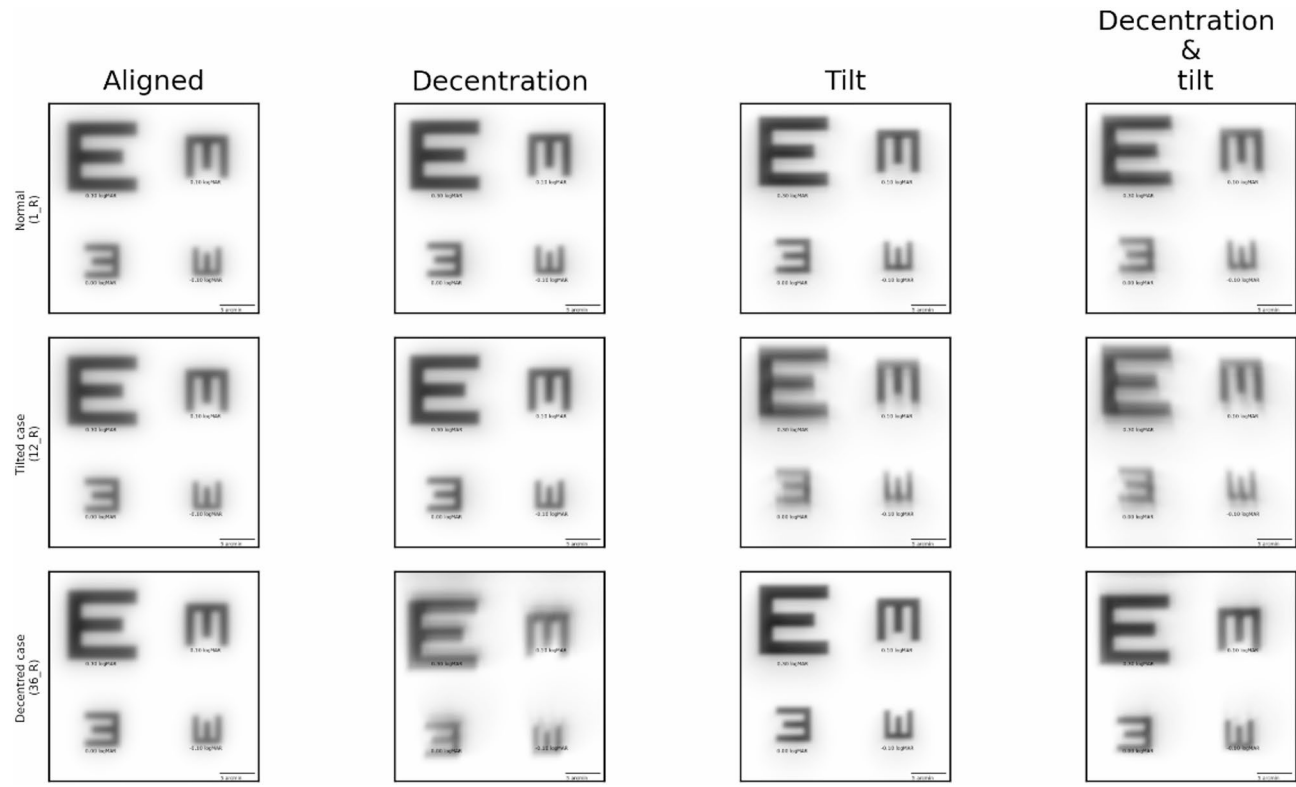


**Fig. 5.** Representation of convolution image in three different cases. The first row shows an eye with IOL tilt and decentration within normal limits. The second row corresponds to the case with maximum IOL tilt, and the third row represents a case with significant IOL decentration.

and complex neural processing, which are not fully accounted for in this study. Another limitation is that no a priori sample size calculation was performed. With 105 eyes, the study has adequate power to detect moderate associations but limited ability to detect small effects. Therefore, while the absence of strong correlations is supported by the data, very small associations cannot be excluded. Another limitation is that the posterior IOL radius was estimated rather than directly measured, as AS-OCT does not reliably capture the posterior surface. This estimation uses the labelled IOL power, which under ISO 11979-2 represents the paraxial power within narrow tolerance limits. Once the anterior radius and central thickness are fixed by OCT, variations within these limits produce only minor adjustments in the inferred posterior curvature and small changes in the downstream ray-tracing results. For this reason, this approximation is not expected to materially affect the conclusions.

Future research should focus on improving the precision of corneal surface modeling, possibly by integrating data from advanced imaging modalities such as Scheimpflug tomography. Additionally, efforts to access and incorporate manufacturer-specific IOL design parameters would enhance the accuracy of simulations. Expanding the model to include polychromatic light and retinal image processing would provide a more comprehensive understanding of the visual impact of IOL misalignment.

Although IOL tilt and decentration induced statistically significant coma aberration in the optical eye model, the analysis of clinical variables did not reveal a consistent relationship with visual outcomes. This suggests that the magnitude of coma induced by the observed levels of misalignment may not be sufficient to significantly impair the best-corrected visual acuity in eyes implanted with the studied aspheric IOL. However, further studies are needed to determine whether the aberrations induced by IOL tilt and decentration have a more relevant impact on visual performance when multifocal IOLs are implanted.

## Data availability

The data that support the findings of this study are available from the corresponding author upon reasonable request.

Received: 13 August 2025; Accepted: 16 December 2025

Published online: 19 December 2025

## References

1. Hoffer, K. J. Astigmatism from lens Tilt. *J. Am. Intraocular Implant Soc.* **11** (1) (1985).
2. Sanders, D. R. & Kraff, M. C. Improvement of intraocular lens power calculation using empirical data. *Am. Intra-Ocular Implant Soc. J.* (1980).

3. Retzlaff, J. A., Sanders, D. R. & Kraff, M. C. Development of the SRK/T intraocular lens implant power calculation formula. *J. Cataract Refract. Surg.* (1990).
4. Atchison, D. A. Refractive errors induced by displacement of intraocular lenses within the pseudophakic eye. *Optom. Vis. Sci.* **66** (3) (1989).
5. Atchison, D. A. & Cooke, D. L. Refractive errors occurring with Tilt of intraocular lenses. *Ophthal. Physiol. Opt.* **44** (1) (2024).
6. Enoch, J. M., Crawford, B. & Nygaard, R. W. Refractive changes induced by intraocular lens Tilt and longitudinal displacement. *Arch. Ophthalmol.* **104** (1) (1986).
7. Pérez-Vives, C., Ferrer-Blasco, T., García-Lázaro, S., Albarrán-Diego, C. & Montés-Micó, R. Optical quality comparison between spherical and aspheric toric intraocular lenses. *Eur. J. Ophthalmol.* **24** (5) (2014).
8. Felipe, A., Artigas, J. M., Díez-Ajenjo, A., García-Domene, C. & Peris, C. Modulation transfer function of a toric intraocular lens: evaluation of the changes produced by rotation and Tilt. *J. Refract. Surg.* **28** (5) (2012).
9. Ferrer-Blasco, T. et al. In vitro optical quality of monofocal aspheric toric intraocular lenses: effect of cylindrical power. *Int. Ophthalmol.* **38** (3) (2018).
10. Atchison, D. A., Suheimat, M., Mathur, A., Lister, L. J. & Rozema, J. Anterior Corneal, posterior Corneal, and lenticular contributions to ocular aberrations. *Invest. Ophthalmol. Vis. Sci.* **57** (13), 5263–5270 (2016).
11. Pérez-Merino, P. et al. In vivo chromatic aberration in eyes implanted with intraocular lenses. *Investig. Ophthalmol. Vis. Sci.* **54** (4) (2013).
12. Pérez-Merino, P. & Marcos, S. Effect of intraocular lens decentration on image quality tested in a custom model eye. *J. Cataract Refract. Surg.* **44** (7) (2018).
13. Weikert, M. P., Golla, A. & Wang, L. Astigmatism induced by intraocular lens Tilt evaluated via ray tracing. *J. Cataract Refract. Surg.* (2018).
14. Wang, L., Guimaraes de Souza, R., Weikert, M. P. & Koch, D. D. Evaluation of crystalline lens and intraocular lens Tilt using a swept-source optical coherence tomography biometer. *J. Cataract Refract. Surg.* **45** (1) (2019).
15. Langenbucher, A., Szentmáry, N., Cayless, A., Wendelstein, J. & Hoffmann, P. Prediction of IOL decentration, Tilt and axial position using anterior segment OCT data. *Graefe's Arch. Clin. Exp. Ophthalmol.* **262** (3) (2024).
16. Ashena, Z., Maqsood, S., Ahmed, S. N. & Nanavaty, M. A. Effect of intraocular lens Tilt and decentration on visual acuity, dysphotopsia and wavefront aberrations. *Vision (Switzerland)* **4** (3) (2020).
17. Madrid-Costa, D. et al. Visual simulation through different intraocular lenses using adaptive optics: effect of Tilt and decentration. *J. Cataract Refract. Surg.* **38** (6) (2012).
18. Lawu, T., Mukai, K., Matsushima, H. & Senoo, T. Effects of decentration and Tilt on the optical performance of 6 aspheric intraocular lens designs in a model eye. *J. Cataract Refract. Surg.* **45** (5) (2019).
19. Pérez-Gracia, J., Varea, A., Ares, J., Vallés, J. A. & Remón, L. Evaluation of the optical performance for aspheric intraocular lenses in relation with tilt and decentrer errors. *PLoS ONE* **15** (5) (2020).
20. Pérez-Gracia, J., Ávila, F. J., Ares, J., Vallés, J. A. & Remón, L. Misalignment and Tilt effect on aspheric intraocular lens designs after a corneal refractive surgery. *PLoS ONE* **15** (2020).
21. Liu, X., Yu, M., Huang, Y., Li, Q. & Wu, W. Intraocular lens Tilt and decentration after cataract surgery with and without primary posterior continuous curvilinear capsulorhexis. *J. Cataract Refract. Surg.* **49** (5) (2023).
22. Taketani, F., Matuura, T., Yukawa, E. & Hara, Y. Influence of intraocular lens Tilt and decentration on wavefront aberrations. *J. Cataract Refract. Surg.* **30** (10) (2004).
23. Robert Iskander, D., Davis, B. A., Collins, M. J. & Franklin, R. Objective refraction from monochromatic wavefront aberrations via Zernike power polynomials. *Ophthalmic Physiol. Opt.* **27** (3), 245–255 (2007).
24. Thibos, L. N., Xin, H., Bradley, A. & Applegate, R. A. Accuracy and precision of objective refraction from wavefront aberrations. *J. Vis.* **4** (4), 329–351 (2004).
25. Campbell, F. W. & Green, D. G. Optical and retinal factors affecting visual resolution. *J. Physiol.* **181** (3) (1965).
26. Krueger, R. R. et al. *Wavefront Customized Visual Correction: The Quest for Super Vision II*. SLACK (2004).

## Acknowledgements

We would like to thank Dr. Larry Thibos for his valuable input and for kindly addressing our questions. We also acknowledge his significant contributions to the field of visual optics, which have been instrumental in shaping the present work.

## Author contributions

GVR drafted the main manuscript and prepared all tables and figures. NAA and IJA contributed to the study design. LGO and ASL were responsible for clinical data collection. MFR supervised and contributed to the optical metrics calculations, guiding GVR. All authors critically reviewed the manuscript and approved the final version for submission.

## Declarations

### Competing interests

The authors declare no competing interests.

### Additional information

**Correspondence** and requests for materials should be addressed to G.V.-R.

**Reprints and permissions information** is available at [www.nature.com/reprints](https://www.nature.com/reprints).

**Publisher's note** Springer Nature remains neutral with regard to jurisdictional claims in published maps and institutional affiliations.

**Open Access** This article is licensed under a Creative Commons Attribution-NonCommercial-NoDerivatives 4.0 International License, which permits any non-commercial use, sharing, distribution and reproduction in any medium or format, as long as you give appropriate credit to the original author(s) and the source, provide a link to the Creative Commons licence, and indicate if you modified the licensed material. You do not have permission under this licence to share adapted material derived from this article or parts of it. The images or other third party material in this article are included in the article's Creative Commons licence, unless indicated otherwise in a credit line to the material. If material is not included in the article's Creative Commons licence and your intended use is not permitted by statutory regulation or exceeds the permitted use, you will need to obtain permission directly from the copyright holder. To view a copy of this licence, visit <http://creativecommons.org/licenses/by-nc-nd/4.0/>.

© The Author(s) 2025